ICARUS **130,** 505–516 (1997)
ARTICLE NO. IS975842

Latitudinal Distribution of O_2 on Ganymede: Observations with the Hubble Space Telescope

Wendy M. Calvin

U.S. Geological Survey, 2255 N. Gemini Dr., Flagstaff, Arizona 86001
E-mail: wcalvin@flagmail.wr.usgs.gov

and

John R. Spencer

Lowell Observatory, 1400 W. Mars Hill, Flagstaff, Arizona 86001

Received February 10, 1997; revised September 15, 1997

To help constrain the spatial variation of oxygen on Jupiter's satellite Ganymede, and hence have more clues to its mode of production and stability, we have obtained spectral data from the Faint Object Spectrograph (FOS) for a single pole-to-pole latitudinal strip, along with several Wide Field Planetary Camera 2 (WFPC2) images in three narrow band visible filters. All observations were made of the trailing hemisphere. In the FOS data we observe both visible absorptions at 0.577 and 0.627 μm, associated with dense-phase oxygen (compressed gases, liquids, or solids). Filter options limited the WFPC2 observations to wavelengths near the weaker oxygen absorption at 0.627 μm. These observations suggest that the dense-phase or dimer oxygen form is predominantly found in equatorial and mid-latitudes. The spectroscopic absorption feature appears in both bright and dark terrains but may be somewhat weaker in dark regions, which is consistent with the smaller mean photon path length in the surface in darker areas. Therefore, the abundance of oxygen appears more dependent on latitude and longitude constraints than surface albedo. At the highest latitudes, where the ratio spectra have a strong upturn toward the blue, the oxygen bands do not appear. This relation suggests that dimer oxygen and ozone (as seen by Galileo) have opposite trends with latitude. Possible causes include competition or variation in the preferred stable form, which depends on temperature, solar ultraviolet flux, and/or surface age; enhancement of O_3 at the poles due to plasma interactions; or viewing geometry effects that reduce the oxygen features at the poles when observed from Earth. The predominantly equatorial feature supports the production of O_2 through plasma bombardment and favors defect trapping over physical adsorption of the dimer molecules in the surface. We briefly consider the implications of Ganymede's magnetosphere for our understanding of O_2 and O_3 distribution on Ganymede. © 1997 Academic Press

INTRODUCTION

Since the identification of the spectral signature of condensed molecular oxygen on Jupiter's satellite Ganymede (Calvin and Spencer 1994, Spencer *et al.* 1995, Calvin *et al.* 1996) a number of exciting new results have surfaced. Noll *et al.* (1996), using the Hubble Space Telescope, discovered the unique ultraviolet signature of ozone on the trailing hemisphere. Recent results from Galileo have shown that Ganymede has an intrinsic magnetic field (Gurnett *et al.* 1996; Kivelson *et al.* 1996) and an atmosphere of atomic hydrogen (Barth *et al.* 1996). The Galileo ultraviolet spectrometer team reports that the ozone absorption feature appears to be concentrated near the polar regions, although a weak signature is observed at the equator with more on the trailing hemisphere (Hord *et al.* 1996, C. Barth personal communication). Hall *et al.* (1996) have suggested the presence of singlet oxygen emission in the polar regions of Ganymede based on observations from the Hubble Space Telescope and interpret this as auroral emission associated with the newly identified magnetic field. Our recent observations from the Hubble Space Telescope in the visible portion of the spectrum were made in order to refine the spatial distribution of the dense-phase oxygen and in light of these new discoveries also have relevance for the photolysis and radiolysis reactions occurring on the surface of Ganymede (Delitsky and Lane 1997; Johnson and Quickenden 1997).

Our initial ground-based data which detected the unique signature of dimer oxygen were constrained to a single spectrum for the entire satellite hemisphere viewed from Earth. Those observations indicated that the oxygen absorption features appeared almost exclusively on the hemi-

0019-1035/97 $25.00

TABLE I
Details of Observations

Date	Start time	Target	Instrument	Geocentric distance	Sub-Earth longitude	Solar phase angle
95/07/06	18:23	Ganymede	FOS	4.49	265	6.7
95/07/14	04:39	Ganymede	WFPC2	4.56	279	7.8
95/07/14	14:21	Callisto	FOS	4.56	270	7.9

Note. Each observation occupied a single HST orbit over a period of about 45 min, with FOS acquisition being done on the previous orbit. Sub-Earth latitude was 2.9S for all observations.

sphere at the antapex of orbital motion also known as the trailing hemisphere (Spencer *et al.* 1995). It was then proposed that this longitudinal variation was consistent with production of the molecule through plasma bombardment of the largely water ice surface (Calvin *et al.* 1996). In order to further define the spatial variability of the oxygen absorption features and to determine if they were related to surface albedo patterns, we made spatially resolved observations with the Hubble Space Telescope (HST) Faint Object Spectrograph (FOS) and Wide Field Planetary Camera 2 (WFPC2) in July of 1995. Here we describe the details of the observation and discuss our results and their implications for both oxygen and ozone on Ganymede.

OBSERVATIONAL DETAILS

We acquired data during three HST orbits in Cycle 5, two each for FOS observations of Ganymede and Callisto and one for WFPC2 images. Table I summarizes the dates, times, and longitudes that were observed. We note that the WFPC2 observation of Ganymede is shifted about 15° in orbital longitude from the FOS observations, though both are within 10° of the central longitude of the trailing hemisphere.

Target acquisition was performed using the Goddard High Resolution Spectrograph in a method designed for extended targets such as the Galilean satellites. This method also allowed imaging the acquisition aperture to confirm pointing. A continuous pole-to-pole scan was then performed with the FOS using the G570H grating, which acquires data from 4571 to 6820 Å at resolving powers of 1300. Constraints on the observation time of moving targets restricted the time available for the pole-to-pole FOS scan to 26 min. The FOS was read out in ''Rapid'' mode to obtain high time resolution with a read time every 30 sec. This resulted in 42 spectra at varying latitudes across the satellite. In order to obtain the highest spatial resolu-

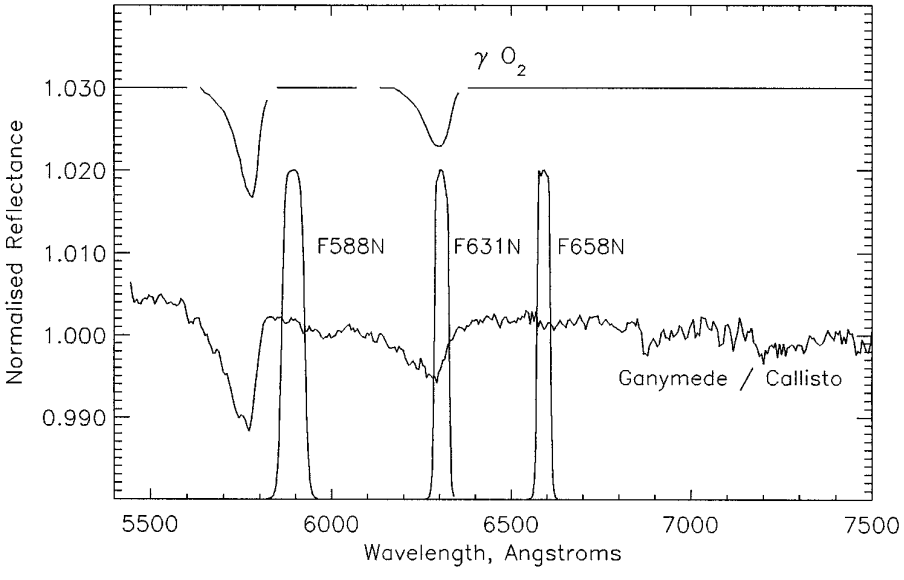

FIG. 1. Comparison of the locations of the Ganymede O_2 bands, seen in a ground-based Ganymede/Callisto disk-integrated ratio spectrum from Fig. 8 of Spencer *et al.* (1995), with the wavelengths of the three HST WFPC2 filters used in this study. The F631N filter overlaps the weaker of the two O_2 bands sufficiently to allow its use for mapping O_2 distribution, while the other two filters provide continuum observations. Also shown is a laboratory spectrum of the γ-form of solid O_2 (Landau *et al.* 1962), showing the good correspondence with the features seen on Ganymede.

TABLE II
WFPC2 Imaging of Ganymede

Filter	Central wavelength, Å	Width, Å	Exposure, s	Frames per CCD position
F588N	5894	49	5.0	2
F631N	6306	31	8.0	3
F658N	6590	29	10.0	2

Note. Filter central wavelengths and widths are taken from the WFPC2 Instrument Handbook, which contains definitions for these quantities.

tion possible we used the smallest aperture, 0.09 arcsec square. This aperture and the continuous scan read out mode resulted in approximately 50% spatial overlap between adjacent latitudinal spectra.

We performed a similar scan across Callisto because the selected aperture was not radiometrically calibrated and because we wanted to use that satellite as a reference standard, observed under the same conditions as Ganymede for best removal of solar spectral features. Ground-based observations indicated that the reflectance spectrum of Callisto exhibits no narrow spectral features in the wavelength range of interest and should therefore be a reasonable standard (e.g., Spencer *et al.* 1995). The scan across Callisto was slightly offset, acquiring one limb but not the other, and resulted in 35 spectra spaced in latitude on that satellite. Unfortunately, the use of the smallest paired aperture, for highest spatial resolution on the satellite, resulted in an automatic object-sky subtraction of the two apertures and reduced our anticipated signal-to-noise. Block averaging of both wavelengths and adjacent latitudes was used to increase the signal-to-noise and is described in the next section. The paired apertures are separated by 2.6 arcsec, assuring that the "sky" aperture is always well off the satellite (diameter of 1.6 arcsec).

A second set of observations was made using the WFPC2 of the HST. No WFPC2 narrowband filter falls within the stronger 5773-Å O_2 band. Instead, we used a filter F631N, which falls mostly within the weaker 6275-Å O_2 band seen in Ganymede's disk-integrated spectrum (Fig. 1). We also used two adjacent narrowband filters, F588N and F658N, to provide continuum images on either side of the band. We obtained three images of Ganymede in the F631N filter and two images in each continuum filter (Table II). We then repeated the sequence with Ganymede at a different location on the CCD, as insurance against flat field errors, for a total of 14 images, all taken on a single orbit. Exposures were made as long as possible, while avoiding saturation to minimize photon noise: peak counts on Ganymede were about 49,000 electrons per pixel in all images.

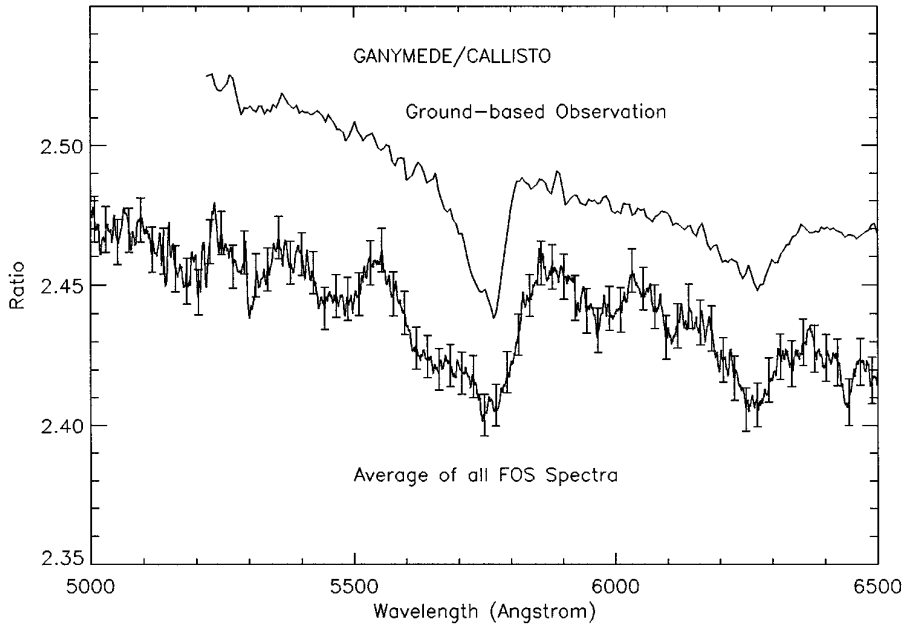

FIG. 2. Ratios of Ganymede/Callisto for the entire spatial extent of the FOS observations compared with the ground-based spectrum of Spencer *et al.* (1995). Both oxygen features at 5770 and 6275 Å are clearly seen in these "disk-integrated" spectra. Error bars indicate the standard deviation of the mean and assume an additional reduction in uncertainty by a factor of 5 from the box-filter average. One would normally expect a reduction by a factor of 8 (square root of 65); however, we believe the actual improvement is lower due to the box-filter average incorporating slopes of absorption features and because we did not account for uncertainty in the average Callisto spectrum. For clarity, errors are only plotted for every 20th channel.

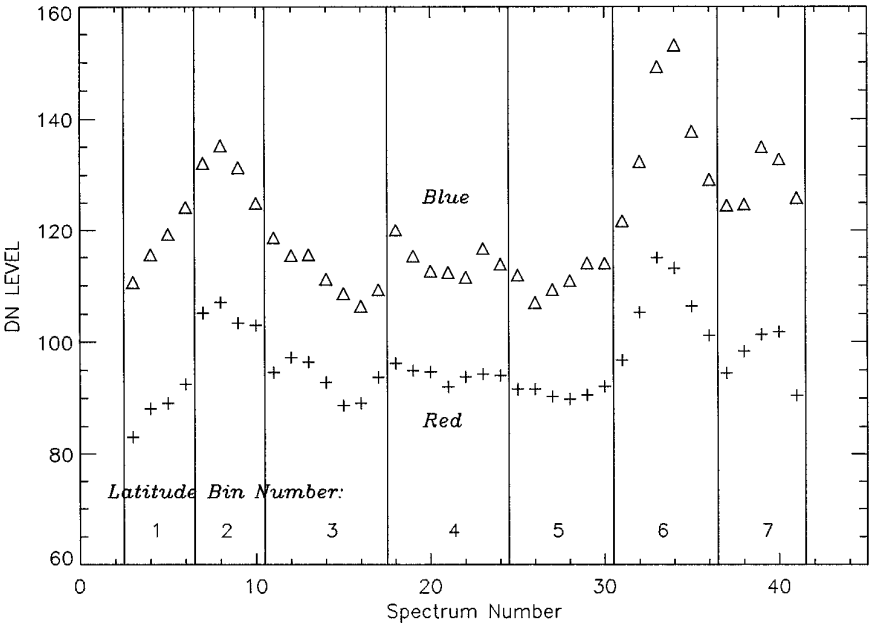

FIG. 3. Plot of digital signal (DN) level (proportional to albedo) with latitude. Spectrum number indicates place in FOS scan from north to south. Triangles represent an average of 12 channels centered on 4745 Å; plusses represent an average of 26 channels around 6384 Å scaled up by a factor of two. Latitude/albedo bins displayed as separate spectra in Figs. 4, 5, and 6 are noted here.

ANALYSIS AND RESULTS

Faint Object Spectrograph

Because the signal-to-noise is low, we first examined spectra which average all the FOS spectra together. For Ganymede, 40 individual spectra were averaged together and then ratioed to the average of 35 Callisto spectra. A box-filter smoothing was then applied and this result is shown in Fig. 2. In practice the width of the box filter is a tradeoff between increased signal-to-noise (S/N) and "smearing" of the long wavelength edge of the oxygen absorption features. A box width of 65 spectral channels (about 70 Å) was chosen as this improved the S/N without strongly affecting the oxygen band shapes. In Fig. 2 both oxygen absorption features are clearly seen, although the strongest feature at 5770 Å appears broader than in our ground-based observation.

We then explored the ability to distinguish spatial variations in the oxygen band strength by binning the spectra into seven latitudinal regions of roughly similar albedo as indicated in Fig. 3. Figure 4 places the approximate trace of our FOS observations onto a projection of the Voyager orange filter global mosaic (Johnson *et al.* 1983, modern digital mosaic data for this and later figures provided by the U.S. Geological Survey, Astrogeology Team). The orthographic projection is done at a sub-Earth latitude of $-2.9°$ and sub-Earth longitude of 265°, thus closely approximating the viewing geometry of the HST-FOS scan. The FOS observations have been overlain at the central longitude by matching the north and south limbs based on signal levels. We do not know precisely how close to the center of the planet the FOS scan actually was, as the target acquisition and observation scans were done on different orbits, with different instruments. Given the close match of the albedo pattern under the assumed projection (Fig. 4) to that actually obtained with the FOS (Fig. 3), we estimate we are off-center no more than an aperture width in either the east or west direction on the planet.

To obtain spectra for each of the latitude bins the individual spectra were first averaged by bin and then ratioed to the average Callisto spectrum. The box-filter smoothing function with a width of 65 channels was again applied to obtain the spectra shown in Fig. 5. This figure shows the FOS spectra as a function of latitude with the most northern spectra at the top. Ratios have been offset so that the spectra are well separated in Fig. 5. The approximate central latitude for the bin is derived from Fig. 4. For reference, also plotted in Fig. 5 is our best ground-based observation. The data are primarily limited by random photon noise with possible minor contributions from incompletely cancelled solar Fraunhofer lines. The estimated total uncertainty (peak to peak) is shown by the error bar in the top right of Fig. 5.

Note that the polar region spectra are significantly brighter at shorter wavelengths. This is expected due to the presence of the polar shroud which increases the blue

TABLE III
Oxygen Band Depth

Latitude bin	O_2 band depth %	Average signal red times 2	Average signal blue
1	0.8	88.2	117.4
2	2.6	104.6	130.9
3	2.0	93.2	112.1
4	2.6	94.2	114.6
5	2.0	91.0	111.1
6	1.4	106.2	137.2
7	0.6	97.2	128.6

albedo over that of non-ice material. We can identify the strongest oxygen feature at 5770 Å in latitude bins 2 (42N), 3 (25N), 4 (EQ), and 5 (20S). The band may also be weakly present in bin 6 (40S). The weaker feature at 6275 Å is also seen at these latitudes. By comparing Figs. 3, 4, and 5 we find that the identification of oxygen is unrelated to albedo, being observed in both dark (latitude bin 3 and 5) and bright (latitude bin 2) regions. The band appears slightly less distinct in the darker regions. This may reflect an actual decrease in abundance or simply the decreased photon path length (higher probability of light absorption) in dark surface materials and is discussed further in the final section.

While the data quality does not warrant detailed reflectance modeling to determine the abundance of O_2, we have classified the band depth in each latitudinal bin. In order to fit the observed oxygen band depth we first derive a second-order polynomial fit to the overall Ganymede/Callisto ratio spectra. This determines a continuum level within the peak-to-peak spectral variation. We next scale the measured transmission spectrum of liquid O_2 from Calvin *et al.* (1995a) to provide an absorption band, i.e., *absorption* = 1 − *transmission* ∗ *scale factor*. This absorption is multiplied by the continuum function to provide the fits shown in Fig. 6, with the oxygen band depths given in Table III. Uncertainties on the band depths are about ±0.2. Because of the fairly high noise level we consider fits with band depths less than 1.5% to be within the noise and therefore do not definitively identify the oxygen feature in the spectra in Fig. 6a. Also presented in Table III is the average DN level for each latitude bin, derived from the values in Fig. 3.

Figures 4 and 6 highlight terrains where the oxygen feature is clearly observed. The strongest feature occurs in equatorial and mid-latitudes, bins 2, 3, 4, and 5. Within the noise level the strength of the feature is the same in bins 2 and 4 and is the same in bins 3 and 5, though the latter are slightly weaker than the first two. The weaker band strength in the darker bins 3 and 5 is probably related to albedo effects, as stated previously. The appearance of the strongest band in both bright and medium bright regions implies that to first order the apperance of the band is not dependent on surface composition. It is interesting to note that the band does not appear at the highest latitudes of either hemisphere, bins 1 (60N) and 7 (65S). In these spectra the ratios are strongly increasing at shorter wavelengths (Fig. 6). The band might be weakly identified in the extremely bright region bin 6 (40S). It is possible that the oxygen is there, but that strong back or surface scattering inhibits deep penetration of photons into the surface and hence the absorption appears weak. Another factor that may reduce the appearance of the absorption at high latitudes is the more oblique viewing geometry.

The fits to the laboratory O_2 feature suggest the possibility that the band shape and center are varying with latitude. Increasing latitude may be related to a longer wavelength for the center of the strongest O_2 feature. The sharp, long-wavelength band edge near 5800 Å appears about 17 Å shorter than in the laboratory O_2 at the equator, the same at 25N and 20S, and 17 Å longer at 42N. Given the high noise level this possibility needs to be confirmed in subsequent observations. The band shape in bins 2, 3, and 5 (42N, 25N, 20S) is broader, and the weak O_2 feature at 6275 Å seems to be shifted to longer wavelengths in bin 2 (42N), though these effects may also be due to random noise spikes. If real, these trends may suggest a temperature dependence or may imply a contribution from ozone at higher latitudes, as will be discussed in the final section. The band asymmetry remains more compatible with that seen in a condensed form of oxygen rather than a high-pressure gas (e.g., Calvin *et al.* 1996).

Wide Field Planetary Camera

An alternative approach to exploring the spatial variation of oxygen was to use ratios of narrowband images of Ganymede's trailing hemisphere within an oxygen absorption and adjacent continua, as described in the previous section on observational details. Dark subtraction and flat fielding of the images were done with standard HST pipeline processing. We then spatially registered all images at each of the two chip positions, using a sinc-function interpolation routine to shift the images by fractional pixels. We used a Simplex algorithm to find the shift that minimized the standard deviation of the difference between pairs of images. Shifts were minor, less than 0.10 pixel to register images taken in the same filter and less than to 0.46 pixel to register images in different filters.

Figures 7A and 7B and 8A and 8B show good agreement between the albedo patterns seen by Voyager and by HST. Comparison of the 5894 and 6590-Å continuum images shows that the darker areas of the surface are redder (Figs. 7B and 8C), as is also apparent at shorter wavelengths in Voyager images (Squyres and Veverka 1982) and as is seen

in our FOS spectra (Figs. 5 and 6). To correct for the wavelength dependence of the continuum images, for each CCD position we created a mean continuum image at 6306 Å by linear interpolation between the long- and short-wavelength continuum images. The disk-integrated spectra (Figs. 1 and 2) show that at least for the disk as a whole, a linear interpolation between 5894 and 6590 Å provides a good approximation to the continuum level at the wavelength of the 6306 Å O_2 band.

Ratios of the 6306 Å image to the interpolated continuum image (Figs. 7C and 7D) are very noisy, but show distinct brightening toward the poles, indicating a weaker O_2 band there, in agreement with the FOS spectral scan. The fact that the polar brightening is seen with Ganymede in each CCD position makes it unlikely that the brightening is an artifact due, for instance, to imperfections in the CCD flat field. When the two O_2 band depth images are registered, coadded, and smoothed further, the latitudinal dependence of band depth becomes clearer (Figs. 7E and 8D). Measured O_2 band depths in the ratio images range from a minimum of zero at high latitudes (white in the images) to about 0.012 in the equatorial regions (dark in the images).

The WFPC2 images thus confirm the FOS spectroscopic result that the O_2 band depths are strongest at low latitudes on Ganymede's trailing side and are weak or absent at high northern and southern latitudes.

IMPLICATIONS

A number of somewhat surprising correlations have been found. First, the appearance of the oxygen feature is to first order, not dependent on the overall albedo, but does not occur in the highest latitudes whose ratios have a strong upturn toward the blue. This latitudinal trend is opposite to that found for ozone (Hord *et al.* 1996, C. Barth personal communication). There may be subtle shifts in band position and shape with latitude, but this needs to be confirmed in subsequent observations. We next consider what these results suggest for the formation, stability, and interplay between oxygen and ozone.

1. Lack of Dense-Phase Oxygen in Polar, "Blue" Spectral Regions

Our observations cannot eliminate the presence of small amounts of either dense-phase oxygen or single oxygen atoms rather than the dimer form in the polar regions. The equatorial concentration of dense-phase oxygen is consistent with the model of Johnson and Jesser (1997), who predict more efficient prodution and trapping of oxygen in bubbles near the equator. Johnson (1985) suggested cold trapping of O_2 on the surface might contribute to the observed polar shroud on Ganymede; however, our observations suggest that this molecule is not the major contributor to the shroud. It appears that O_3 is either readily photolyzed at the equator, resulting in the dominant spectral signature of O_2 there, or is enhanced via plasma processes at the poles. It may be that the polar shroud consists in part of O_3, and the polar ozone may contribute to the observed polar oxygen emission. The polar shroud is inferred to be younger than the underlying terrain (e.g., Hillier *et al.* 1996). It may be that the younger surface has not had sufficient time to build up enough oxygen so that it becomes spectrally apparent or that the photon path length in these bright surfaces is shorter due to scattering and so the oxygen feature is not apparent. The ultraviolet signature of ozone is exceptionally strong so small quantities may be more readily seen. We have HST Cycle 7 time with the Space Telescope Imaging Spectrometer (STIS) which may help resolve these issues.

2. Independence of Band Depth and Albedo

These HST results do not necessarily indicate any change in the abundance of oxygen with albedo. The strongest features occur in both bright and medium bright regions. Small differences between brighter and darker areas (latitude bins 2, 3, 4, and 5) can be explained either by abundance variations or by the smaller depth of penetration of light in dark areas. The very weak suggestion of an O_2 absorption in the brightest region (bin 6) may also be related to surface scattering of photons and lack of light penetration into the surface. This suggests that the presence of O_2 is not directly linked to surface composition nor to the amount of non-water-ice material in the surface.

FIG. 4. Orthographic projection of Voyager orange filter ($\lambda = 0.59\ \mu$m) global mosaic. Central longitude is 265° on the planet. Overlain in small white squares is the approximate location of the center of individual FOS spectra. The white squares substantially undersample the actual aperture size on the planet so that they are clearly seen. The colored rectangles indicate latitude bins presented in Fig. 3. The width of the colored areas is close to the actual aperture width of the observations.

FIG. 5. FOS spectra of seven latitude/albedo bins as noted in Figs. 3 and 4. These ratios to Callisto are scaled independently with a simple offset between spectra in order to be well separated on the plot; they do not reflect actual albedo levels. Bin 1 is offset 0.5, bin 3 is offset 0.2, and bin 6 is offset −0.5; others are not offset. The equatorial bin is labeled "EQ." For reference, the best ground-based spectrum is labeled "GB." The approximate error bar in the top right is the total estimated uncertainty and is calculated as twice the average standard deviation of the mean for latitude bin 4, again reduced by a factor of 5 for the box-filter average as described for Fig. 2.

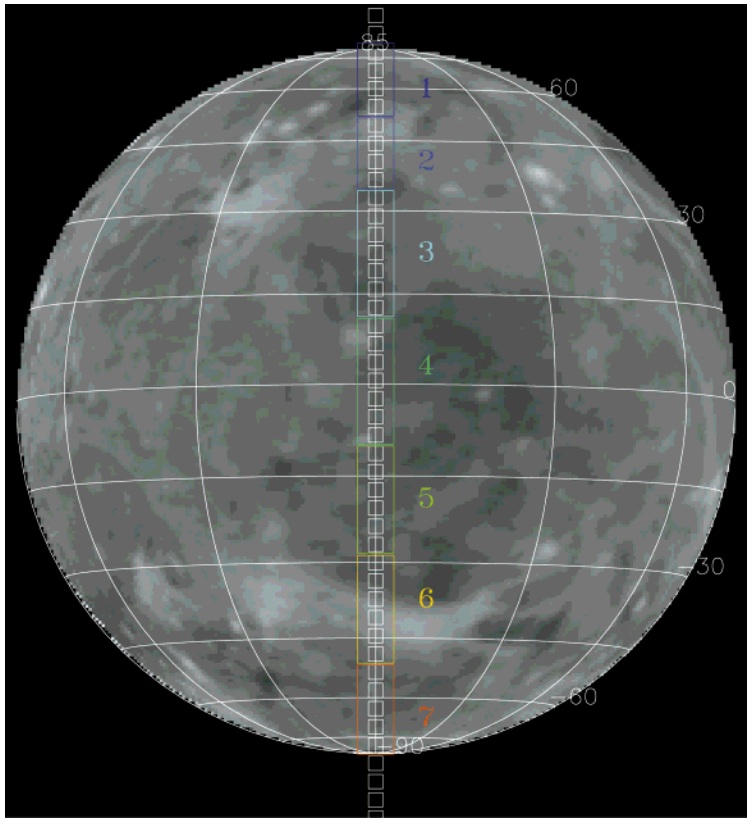
1
2
3
4
5
6
7
60
30
0
30
60

4

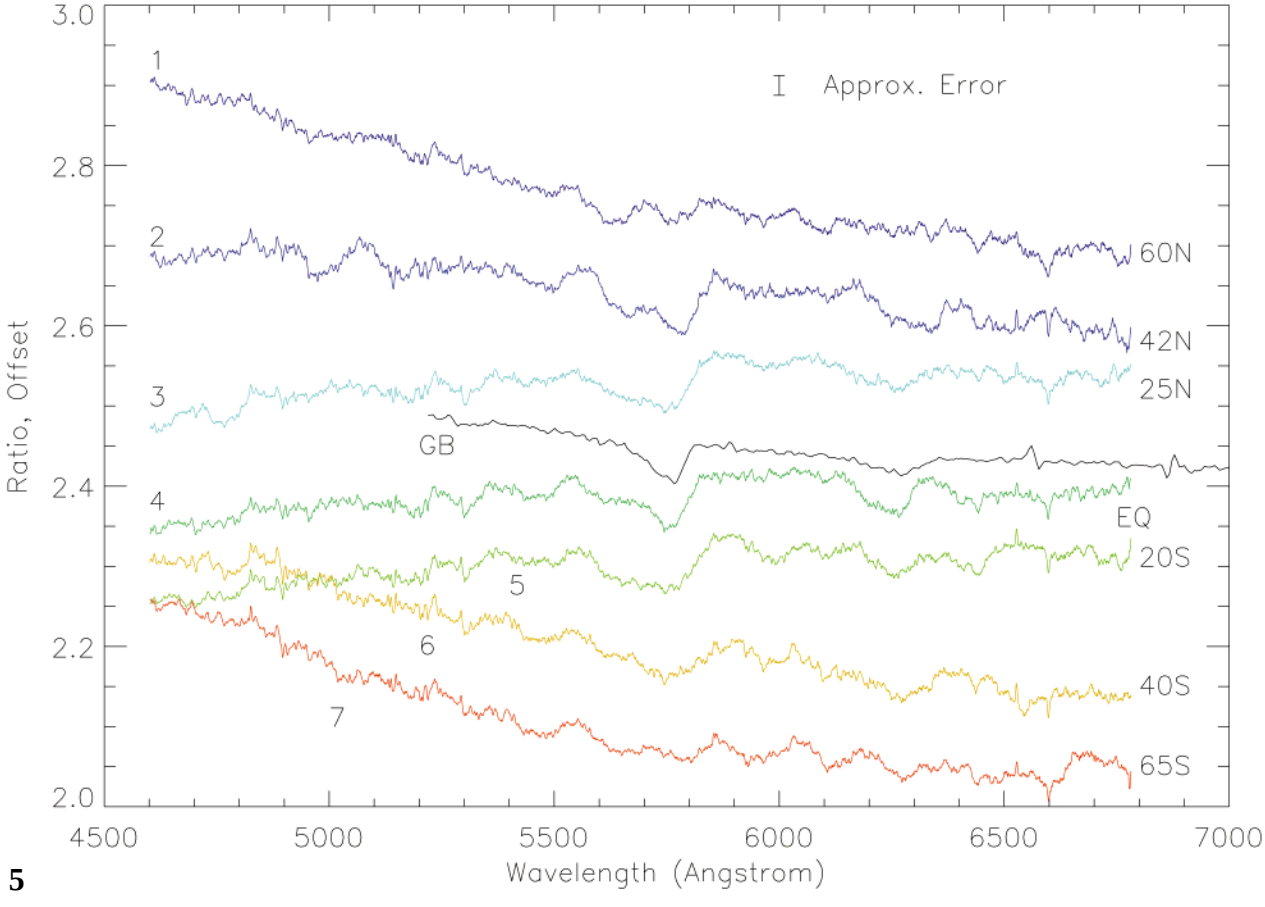
I Approx. Error
1
2
3
4
5
6
7
60N
42N
25N
GB
EQ
20S
40S
65S
Ratio, Offset
Wavelength (Angstrom)
3.0
2.8
2.6
2.4
2.2
2.0
4500
5000
5500
6000
6500
7000

5

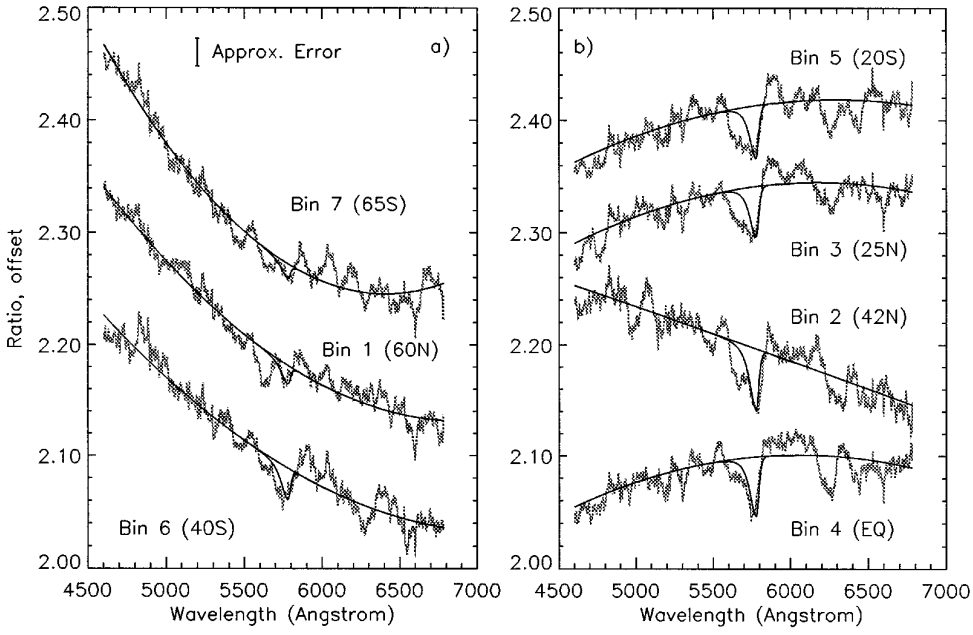

FIG. 6. Fits to the oxygen band depth in each of the seven latitude bins. Fitting procedure described in the text. The continuum level (second-order polynomial fit to each spectrum) and the continuum multiplied by the oxygen feature are both plotted in solid lines. The observed spectra are presented in a stippled line pattern. Spectra are arranged according to oxygen band depth (see also Table III), with smallest band depths on the top of both (a) and (b). For spectra in (a), an oxygen band cannot be definitively identified above the noise level. Offsets are as follows: bin 7 +0.2, bin 1 −0.065, bin 6 −0.6, bin 5 +0.1, bin 3 none, bin 2 −0.45, bin 4 −0.3. The error bar in (a) is calculated the same as in Fig. 5.

3. Possible Shift in Band Center and Shape with Latitude

Noll *et al.* (1996) recently identified a broad absorption band in the ultraviolet, characteristic of ozone. The Galileo ultraviolet spectrometer has recently reported the presence of this feature weakly at equatorial regions with more on the trailing hemisphere and with a marked increase at the poles (Hord *et al.* 1996, C. Barth personal communication). As discussed by Calvin *et al.* (1996) ozone has distinctive absorption features in the visible that are much broader and shifted to longer wavelengths than the oxygen features. Distinct ozone features were not observed in our ground-based telescopic observations and are not seen in the FOS spectra. However, latitude bins 3 and 5 may have a slightly different band shape from that of bins 2 and 4 (Fig. 5), and there may be a trend toward a longer wavelength band center at higher latitudes, as discussed previously. The data quality is limited and we cannot state this unambiguously. Vaida *et al.* (1989) present spectra of ozone in an oxygen matrix, and the visible absorption feature is a distorted combination of the absorption features of both pure O_2 (Calvin *et al.* 1995a) and O_3 (Inn and Tanaka 1953). This may contribute to the possible shifts in band shape and center seen in our latitudinally resolved spectra. It should be noted that ozone has an additional absorption feature at 6000 Å that is not apparent in the ground-based spectra, but might be weakly suggested in the FOS single average (Fig. 2) or in some latitude bins (Fig. 6).

4. Residence in the Surface

Work by Sieveka and Johnson (1982) proposed that molecules eroded and redistributed by plasma bombardment should have a net loss in the equatorial region and a net gain in mid-latitudes. This study was specifically for water-ice but the results should be generally, if not quantitatively, applicable for the redistribution of oxygen. The observed equatorial abundance of oxygen favors trapping of oxygen in damaged lattice sites or in plasma produced "bubbles" (Calvin *et al.* 1996; Johnson and Jesser 1997) rather than physical adsorption after thermal or plasma redistribution. Recent lab measurements by Vidal *et al.* (1997) suggest that oxygen co-condensed with water at low temperatures (26K) will precipitate into aggregates, rather than dissolving uniformly in a thin water ice film. Upon heating they find a large amount of the oxygen desorbs at 45K and leads to the disappearance of the visible absorption features by 100K. However, they find that substantial amounts of oxygen (up to 20%) remain in the thin films at temperatures greater than 100K, with secondary thermal desorption peaks occurring at 147 and 165K. Vidal *et al.* interpret the disappearance of the visible absorption features by 100K in their laboratory thin films to mean that dense phase oxygen on Ganymede must be in either a very cold subsurface layer or an atmospheric "haze." They suggest both of these to be "diurnally" driven; that is, as the trailing hemisphere moves into sunlight the cold oxygen

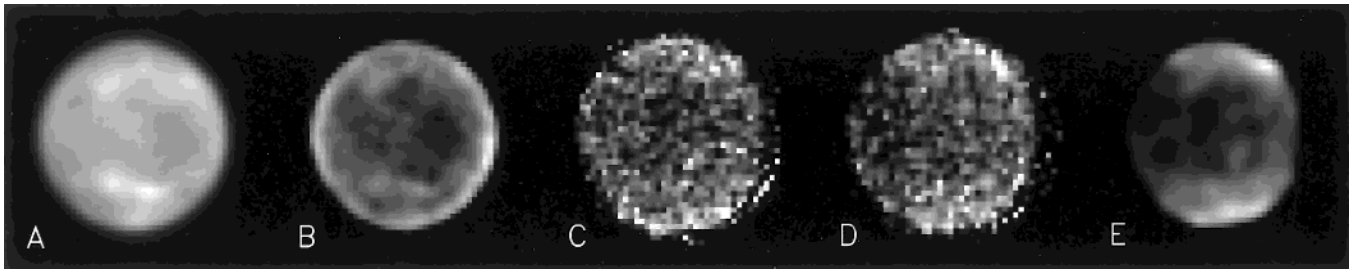

FIG. 7. HST images of Ganymede, north at the top. (A) Continuum image of Ganymede, without contrast enhancement. (B) 5894/6590 Å continuum ratio image, showing the correlation between low albedo regions and red regions, which appear darker in this ratio. The dynamic range of the image, from black to white, is 7%. The bright limb is an artifact of HST's wavelength-dependent point-spread function. (C) 6306 Å/continuum ratio image, first CCD position. Darker areas have a stronger 6300 Å O_2 absorption band. (D) 6306 Å/continuum ratio image, second CCD position. Frames C and D provide two independent observations of the distribution of the O_2 band strength. (E) The average of frames C and D, smoothed by a Gaussian filter to reduce noise. Black corresponds to a 6300 Å O_2 band depth of 0.014, and white corresponds to a band depth of zero.

layer trapped at night is sublimed. Problems with the haze model include that the atmosphere of Ganymede is very tenuous and it is not clear that it can support an optically thick haze, and there is no evidence of such hazes from Voyager or Galileo images. They justify a possible cold subsurface layer with brightness temperatures from 6-cm radiometry, yet this would require that optical photons also probe to depths of 6 to 10 cm in order to see this cold subsurface layer. Viewing these depths at visible wavelengths is inconsistent with estimates of the visible optical path length in the surface on the order of 1 cm (e.g., Calvin *et al.* 1996). In addition, we observe the features predominantly when the trailing hemisphere is in full sunlight, not at ''morning'' or ''evening'' limbs (Spencer *et al.* 1995, Fig. 8). Therefore, we find the explanation of Vidal *et al.* (1997) unlikely. Rather, we interpret the disappearance of the absorption features from 100K thin films to suggest that laboratory conditions cannot directly emulate those on the surface of Ganymede, and clearly the long-term stability of dense-phase oxygen in the surface remains an open question.

5. *Implications of Ganymede's Magnetosphere*

The discovery of Ganymede's magnetosphere by Galileo (Kivelson *et al.* 1996, Gurnett *et al.* 1996) has interesting implications for the generation of O_2 and O_3 on Ganymede's surface, particularly the trailing-hemisphere concentration of O_2 (Spencer *et al.* 1995) and O_3 (Noll *et al.* 1996, Hord *et al.* 1996). Johnson and Jesser (1997) and Calvin *et al.* (1996) state that the heavy ion component (rather than photons or fast protons) should dominate in the production of oxygen on Ganymede. Yet, high-energy heavy ions have only a modest leading/trailing (L/T) asymmetry (Pospieszalska and Johnson 1989). The addition of a magnetosphere with a dipole moment anti-parallel to Jupiter's (Kivelson *et al.* 1996) should prevent low energy ions (with a pronounced L/T asymmetry) from reaching the equator but also enhance particles reaching the leading hemisphere (e.g., Wolff and Mendis 1983). If the L/T asymmetry is due to magnetospheric bombardment, the following explanations should be considered:

(i) If high-energy ions are primarily responsible for the production of oxygen, they must act over sufficient time to build up a pronounced L/T asymmetry.

(ii) If production of oxygen rapidly reaches the observed steady state, low-energy (less than tens of keV) ions must be able to penetrate the magnetosphere to the surface, and if they are deflected by the magnetosphere the deflection is insufficient to remove their pronounced L/T asymmetry.

(iii) The magnetosphere is not constant and is sometimes weak enough for low-energy ions to penetrate to the surface.

(iv) O_2 and O_3 are produced more-or-less equally on both hemispheres of Ganymede, by bombardment by high-energy ions that can penetrate the magnetosphere, or perhaps by solid-state photochemistry (either of which would explain the equatorial concentration of the O_2 reported in this paper). O_2 and O_3 are then preferentially removed or hidden from the leading hemisphere, most likely by micrometeorite bombardment. Micrometeorite impacts should be concentrated on the leading side for particles originating outside the Jovian system (Shoemaker and Wolfe 1982), though the smallest and most numerous particles have orbits that are strongly perturbed by electromagnetic forces (e.g., Hamilton and Burns 1993, Horanyi *et al.* 1993), and their satellite impact geometry is less certain (Hill and Mendis 1981). Micrometeorite impacts could allow escape of the oxygen by local heating of the surface or could perhaps bury it more rapidly than it is formed: the top 10-μm of Ganymede's surface may be turned over by micrometeorite gardening in less than 100 years (Spencer 1987).

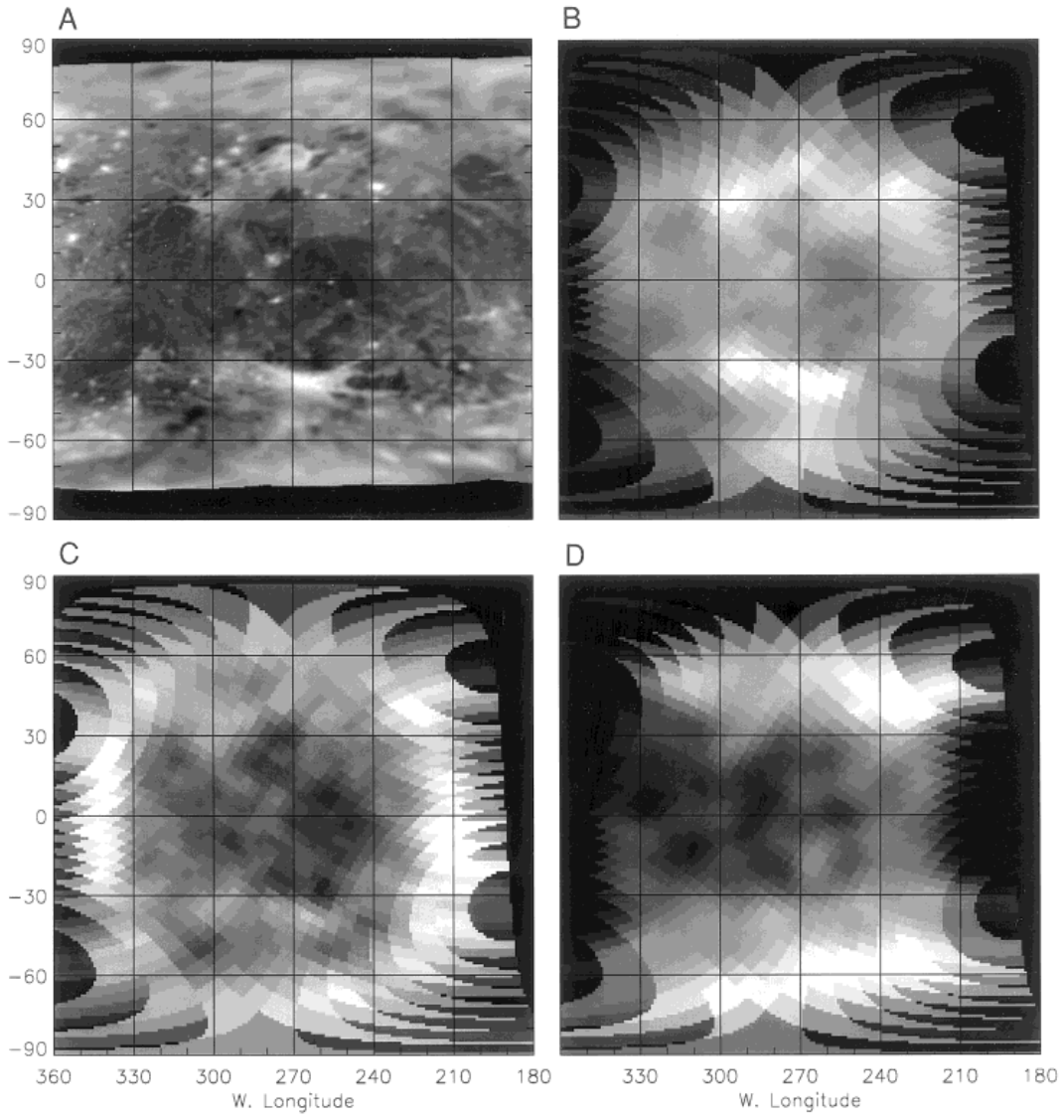

FIG. 8. Maps of Ganymede's trailing hemisphere, all covering the same area. The geometric pattern near the edges of the HST maps is an artifact of the large HST pixel size. (A) Voyager clear-filter mosaic. (B) HST continuum image, interpolated to 6306 Å, showing the good agreement with Voyager in the nature and location of albedo patterns. (C) HST short-wavelength/long-wavelength continuum ratio map, showing the greater redness of the darker regions. Scaling is the same as Fig. 7B, and the bright margin is the same artifact seen in Fig. 7B. (D) Map of HST oxygen band depth, from Fig. 7E, showing the strong latitudinal dependence of band strength. Darker areas have a stronger O_2 band, with the same scaling as Fig. 7E. Fine structure on the 10° lat./lon. scale is probably noise.

Improved modeling of surface and magnetospheric processes, and better observations of the O_2 and O_3 spatial distribution, should help to distinguish between these models.

6. *Implications for Other Molecules*

Some work has been done regarding $O_2/O_3/H_2O$ systems with respect to polar aerosols and the annual destruction of terrestrial ozone (e.g., Sedlacek and Wight 1989). Other materials that are expected to be either intermediate or end products of photochemical processes include HO_2 and H_2O_2 (see also Matich *et al.* 1993). In particular, H_2O_2 has been found to be stable in Antarctic ice cores for as long as several thousand years (Sigg and Neftel 1988). Peroxide production is strongly related to the availability of sunlight and may assist in the destruction of ozone (e.g., de Serves 1994), so the observed distribution of O_2 and O_3 on Ganymede might suggest that H_2O_2, if present, may also be concentrated in the equatorial regions. While these peroxides have no visible absorption features, and apparently only weak absorption in the UV, at least H_2O_2 is distin-

guished from water-ice in the spectral range longer than 3 μm by strong features near 3.08 and 3.571 μm, with shifts to longer wavelengths when peroxide is isolated in Ar or N_2 (Lannon *et al.* 1971). Calvin *et al.* (1995b) noted possible absorptions on the trailing hemisphere of Ganymede near 3.5 and 3.6 μm but were unwilling to interpret these without subsequent confirmation. Also of particular interest is the terrestrial finding that H_2O_2 is primarily responsible for oxidation of SO_2 in a liquid state and the generation of sulfuric acid (e.g., Penkett *et al.* 1979, Calvert *et al.* 1985). On Ganymede it may be possible that similar mechanisms operate and result in the formation of sulfate-bearing minerals; this may help to explain the lack of pure SO_2 on Ganymede. The data from Galileo NIMS should help in identifying these other expected molecules.

ACKNOWLEDGMENTS

We thank Bob Johnson for numerous conversations regarding plasma/ice interactions and Keith Noll and Charles Barth for input regarding the presence and location of ozone. Thanks to Bonnie Buratti, Bob Johnson, Hugh Kieffer, and Jeff Kargel for reviews of the original manuscript. Support for this work was provided by NASA through Grant GO-6029.03-94A from the Space Telescope Science Institute, which is operated by the Association of Universities for Research in Astronomy, Inc., under NASA Contract NAS5-26555. Additional funding support for W.M.C. was provided by NASA Planetary Geology and Geophysics Program, Order W18,962.

REFERENCES

Barth, C. A., and 8 colleagues 1996. Galileo ultraviolet spectrometer observations of atomic hydrogen in the atmosphere of Ganymede (abstract). *EOS Suppl.* **77,** F430.

Calvin, W. M., and J. R. Spencer 1994. Identification of O_2 on Ganymede. *Bull. Am. Astron. Soc.* **26,** 1159. [Abstract]

Calvin, W. M., R. H. Brown, and V. G. Anicich 1995a. Transmission measurements of condensed O_2 in the visible and near infrared. *Bull. Am. Astron. Soc.* **27,** 1165. [Abstract]

Calvin, W. M., R. N. Clark, R. H. Brown, and J. R. Spencer 1995b. Spectra of the icy Galilean satellites from 0.2- to 5-μm: A compilation, new observations and a recent summary. *J. Geophys. Res.* **100,** 19,041–19,048.

Calvin, W. M., R. E. Johnson, and J. R. Spencer 1996. O_2 on Ganymede: Spectral characteristics and plasma formation mechanisms. *Geophys. Res. Lett.* **23,** 673–676.

Calvert, J. G., A. Lazrus, G. L. Kok, B. G. Heikes, J. G. Walgea, J. Lind, and C. A. Cantrell 1985. Chemical mechanisms of acid generation in the troposphere. *Nature* **317,** 27–35.

Delitsky, M. L., and A. L. Lane 1997. Chemical schemes for surface modification of icy satellites: A road map. *J. Geophys. Res.* **102,** 16,385–16,390.

de Serves, C. 1994. Gas phase formaldehyde and peroxide measurements in the Arctic atmosphere. *J. Geophys. Res.* **99,** 25,391–25,398.

Gurnett, D. A., W. S. Kurth, A. Roux, S. J. Bolton, and C. F. Kennel 1996. Evidence for a magnetosphere at Ganymede from plasma-wave observations by the Galileo spacecraft. *Nature* **384,** 535–537.

Hall, D. T., P. D. Feldman, D. F. Strobel, and M. A. McGrath 1996. Far-ultraviolet emissions from Ganymede and Europa. *Bull. Am. Astron. Soc.* **28,** 1071. [Abstract]

Hamilton, D. P., and J. A. Burns 1993. Ejection of dust from Jupiter's gossamer ring. *Nature* **364,** 695–699.

Hill, J. R., and D. A. Mendis 1981. Charged dust in the outer planetary magnetospheres. III. Satellite impact geometries. *Moon Planets* **25,** 427–436.

Hillier, J., P. Helfenstein, and J. Veverka 1996. Latitude variations of the polar caps on Ganymede. *Icarus* **124,** 308–317.

Horanyi, M., G. Morfill, and E. Grün 1993. Mechanism for the ejection of dust form Jupiter's magnetosphere. *Nature* **363,** 144–146.

Hord, C. W., and 9 colleagues 1996. Galileo ultraviolet spectrometer observations of the albedo of Ganymede. *EOS Suppl.* **77,** F441. [Abstract]

Inn, E. C. Y., and Y. Tanaka 1953. Absorption coefficient of ozone in the ultraviolet and visible regions. *J. Opt. Soc. Am.* **43,** 870–873.

Johnson, R. E. 1985. Polar frost formation on Ganymede. *Icarus* **62,** 344–347.

Johnson, R. E., and W. A. Jesser 1997. O_2/O_3 microatmospheres in the surface of Ganymede. *Astrophys. J.* **480,** L79–L82.

Johnson, R. E., and T. I. Quickenden 1997. Photolysis and radiolysis of water ice on outer Solar System bodies. *J. Geophys. Res.* **102,** 10985–10996.

Johnson, T. V., L. A. Soderblom, J. A. Mosher, G. E. Danielson, A. F. Cook, and P. Kupperman 1983. Global multispectral mosaics of the icy Galilean satellites. *J. Geophys. Res.* **88,** 5789–5805.

Kivelson, M. G., K. K. Khurana, C. T. Russell, R. J. Walker, J. Warnecke, F. V. Coroniti, C. Polanskey, D. J. Southwood, and G. Schubert 1996. Discovery of Ganymede's magnetic field by the Galileo spacecraft. *Nature* **384,** 537–541.

Landau, A., E. J. Allin, and H. L. Welsh 1962. The absorption spectrum of solid oxygen in the wavelength region from 12,000 to 3300 Å. *Spectrochim. Acta* **18,** 1–19.

Lannon, J. A., F. D. Verderame, and R. W. Anderson, Jr. 1971. Infrared spectrum of solid and matrix-isolated H_2O_2 and D_2O_2. *J. Chem. Phys.* **54,** 2212–2223.

Matich, A. J., M. G. Bakker, D. Lennon, T. I. Quickenden, and C. G. Freemen 1993. O_2 luminescence from UV-excited H_2O and D_2O ices. *J. Phys. Chem.* **97,** 10539–10553.

Noll, K. S., R. E. Johnson, A. L. Lane, D. L. Domingue, and H. A. Weaver 1996. Detection of ozone on Ganymede. *Science* **273,** 341–343.

Penkett, S. A., B. M. R. Jones, K. A. Brice, and A. E. J. Eggleton 1979. The importance of atmospheric ozone and hydrogen peroxide in oxidising sulphur dioxide in cloud and rainwater. *Atmos. Environ.* **13,** 123–137.

Pospieszalska, M. K., and R. E. Johnson 1989. Magnetospheric ion bombardment profiles of satellites: Europa and Dione. *Icarus* **78,** 1–13.

Sedlacek, A. J., and C. A. Wight 1989. Photochemistry of solid ozone. *J. Phys. Chem.* **93,** 509–511.

Shoemaker, E. M., and R. F. Wolfe 1982. Cratering time scales on the Galilean satellites. In *Satellites of Jupiter* (D. Morrison, Ed.), pp. 277–339. Univ. of Arizona Press, Tucson.

Sieveka, E. M., and R. E. Johnson 1982. Thermal and plasma-induced molecular redistribution on the icy satellites. *Icarus* **51,** 528–548.

Sigg, A., and A. Neftel 1988. Seasonal variations in hydrogen peroxide in polar ice cores. *Ann. Glaciol.* **10,** 157–162.

Spencer, J. R. 1987. Thermal segregation of water ice on the Galilean satellites. *Icarus* **69,** 297–313.

Spencer, J. R., W. M. Calvin, and M. J. Person 1995. CCD spectra of the Galilean satellites: Molecular oxygen on Ganymede. *J. Geophys. Res.* **100,** 19,049–19,056.

Squyres, S. W., and J. Veverka, 1982. Color photometry of surface features on Ganymede and Callisto. *Icarus* **52,** 117–125.

Wolff, R. S., and D. A. Mendis 1983. On the nature of the interaction of the jovian magnetosphere with the icy Galilean satellites. *J. Geophys. Res.* **88,** 4749–4769.

Vaida, V., D. J. Donaldson, S. J. Strickler, S. L. Stephens, and J. W. Birks 1989. A reinvestigation of the electronic spectra of ozone: Condensed-phase effects. *J. Phys. Chem.* **93,** 506–508.

Vidal, R. A., D. Bahr, R. A. Baragiola, and M. Peters 1997. Oxygen on Ganymede: Laboratory studies. *Science* **276,** 1839–1842.